Young Scientists Summer Program

Optimization of the IIASA's FLAM model to represent forest fires in South Korea

Hyun-Woo Jo (endeavor4a1@gmail.com)

Approved by:

Mentor(s): Dr. Andrey Krasovskiy (krasov@iiasa.ac.at) & Dr. Florian Kraxner (kraxner@iiasa.ac.at)
Program: Agriculture, Forestry, and Ecosystem Services (AFE) – Biodiversity and Natural Resources (BNR)
Date: 30 Sep. 2022

This report represents the work completed by the author during the IIASA Young Scientists Summer Program (YSSP) with approval from the YSSP mentor.

It was finished by _____ and has not been altered or revised since.

Mentor signature:

Dr. Andrey Krasovskiy
Research Scholar
Agriculture, Forestry, and Ecosystem Services (AFE)
Biodiversity and Natural Resources Program (BNR)

Table of contents

Abstract

Global risk of forest fires is amplified by the climate change driven heat waves, leading to more intensive biomass burning, which create a vicious cycle by accelerating the climate change. Despite of the growing risk of forest fires, a response system in South Korea, where more than 60% of its land is forest, is still focusing on posterior measures. To improve preventive measures, forest fire model needs to be developed for assessment of future risks of forest fires and burned areas. In this context, this study aims at optimization of the IIASA's FLAM – a processed based model integrating both biophysical and human impacts – to the environment of South Korea for projecting the pattern and scale of future forest fires. The following model developments were performed in the study: 1) optimization of probability algorithms in FLAM, including ignition probabilities conditional on population density, lightning frequency, and fuel taking into account distance to cropland, based on the national GIS data downscaled to 1 km^2, and 2) improvement of fuel moisture computation by adjusting Fine Fuel Moisture Code (FFMC) used by FLAM to represent feedbacks with vegetation; this was done by fitting soil moisture to the daily remote sensing data, 3) deeper look at the fire frequency in addition to areas burned simulated by FLAM. Our results show that the optimization has considerably improved the modelling of seasonal pattern of forest fire frequency. After optimization Pearson's correlation coefficient between monthly predictions and observations from national statistics was improved from 0.171 in non-optimized version to 0.893 in the optimized version of FLAM. These findings imply that even though FLAM already contained main algorithms for interpreting biophysical and human impact on forest fire at a global scale, they were applicable to South Korea only after optimization of all its modules. In addition, as the optimization succeed to reproduce the national specific pattern of forest fire, it should be followed by the research for developing adaptation strategies corresponding to the projected risks of future forest fires.

About the author

Hyun-Woo Jo received B.S. degree in environmental science and ecological engineering from Korea University, Republic of Korea, in 2018, where he is currently pursuing the M.S./Ph.D. integrated degree in environmental planning and landscape architecture. His research interest includes processing remote sensing data with deep-learning techniques in the field of agro-forestry and integrating data science concepts with field specific domain knowledge. During his degree course, he was involved in Horizon2020-EOPEN project and developed deep-learning based rice paddy detection model which is integrated on the platform. He is also involved in Horizon2020-CALLISTO project where he is researching on deep-learning based agricultural monitoring to support decision making. (Contact: endeavor4a1@gmail.com)

Acknowledgments

Introduction & Background

Introduction

As a part of international efforts toward Net Zero, the need of preserving forests, the carbon absorption sources is greater than ever. In particular, a risk of forest fire has been increased by the climate change driven heat waves (Sutanto *et. al.*, 2020), and forest fires create a vicious cycle of accelerating the climate change (Clark *et. al.*, 1996; Randerson *et. al.*, 2006). To decouple the cycle and be resilient to the disaster, both short-term response and long-term objective are required (Engle *et. al.*, 2014). However, a response system in South Korea is much more focused on short-term warning or posterior measures rather than a long-term projection, which is essential for establishing long-term sustainable objectives.

Diverse research efforts have been widely conducted to project forest fire in climate change scenarios, and increasing temperature and dryness were common threat for amplifying the forest fire risk (Varela et. al., 2019; Jadmiko et. al., 2017). Meanwhile, social and biophysical characteristics of each region has to be considered to project forest fire as it is significantly affected by both spatial and temporal patterns of regional forest fire dynamics (Gavin *et. al.*, 2007; Fernandez-Anez *et. al.*, 2021).

In this context, this study aims to develop a forest fire model in South Korea on the basis of IIASA's FLAM, which already contains main algorithms for interpreting social and biophysical factors on forest fire. To represent national specific patterns of forest fire and contribute in establishing local scale objectives with precise projection, the development includes 1) optimization of probability algorithms in FLAM, including ignition probabilities conditional on population density, lightning frequency, and fuel taking into account distance to cropland, based on the national GIS data downscaled to 1km2, and 2) improvement of soil moisture computation by adjusting Fine Fuel Moisture Code (FFMC) used by FLAM to represent feedbacks with vegetation; this was done by fitting soil moisture to the daily remote sensing data, 3) deeper look at the fire frequency in addition to areas burned simulated by FLAM.

Background

With more than 60% of its land covered with forest, South Korea is suffering from forest fire with 562 forest fire events burning 1,863 ha annually for recent 5 years in average (Korea Forest Service, 2022). Located at the peninsular in the mid-latitude of Eastern Asia, South Korea is affected by a warm monsoon climate which leads to great seasonal climate variation; more than 60% among 1,200mm of annual precipitation concentrated in hot rainy summer season while dry from winter to spring, and both warm and dry weather makes spring extremely vulnerable to forest fire (Lim *et. al.,* 2019). Therefore, most of the forest fire occurs in spring from Feb. to Apr. because of the combination of dry and warm weather through the season developing a large portion of mistake ignitions by human to forest fire, especially near the Seoul and south-eastern metropolitan areas (Fig. 1). In addition, the mountain chain developed from the north to the south at the east of Korean Peninsula affects to the humidity. Dry wind from the north east continent in spring becomes much drier passing over the mountain chain and cause large scale forest fires at the east coastal area (Lee & In, 2009). Based on the

correlation between historical meteorology and recorded forest fire, both frequency and scale of forest fire in South Korea are expected to be increased by the climate change (Sung *et. al.*, 2010).
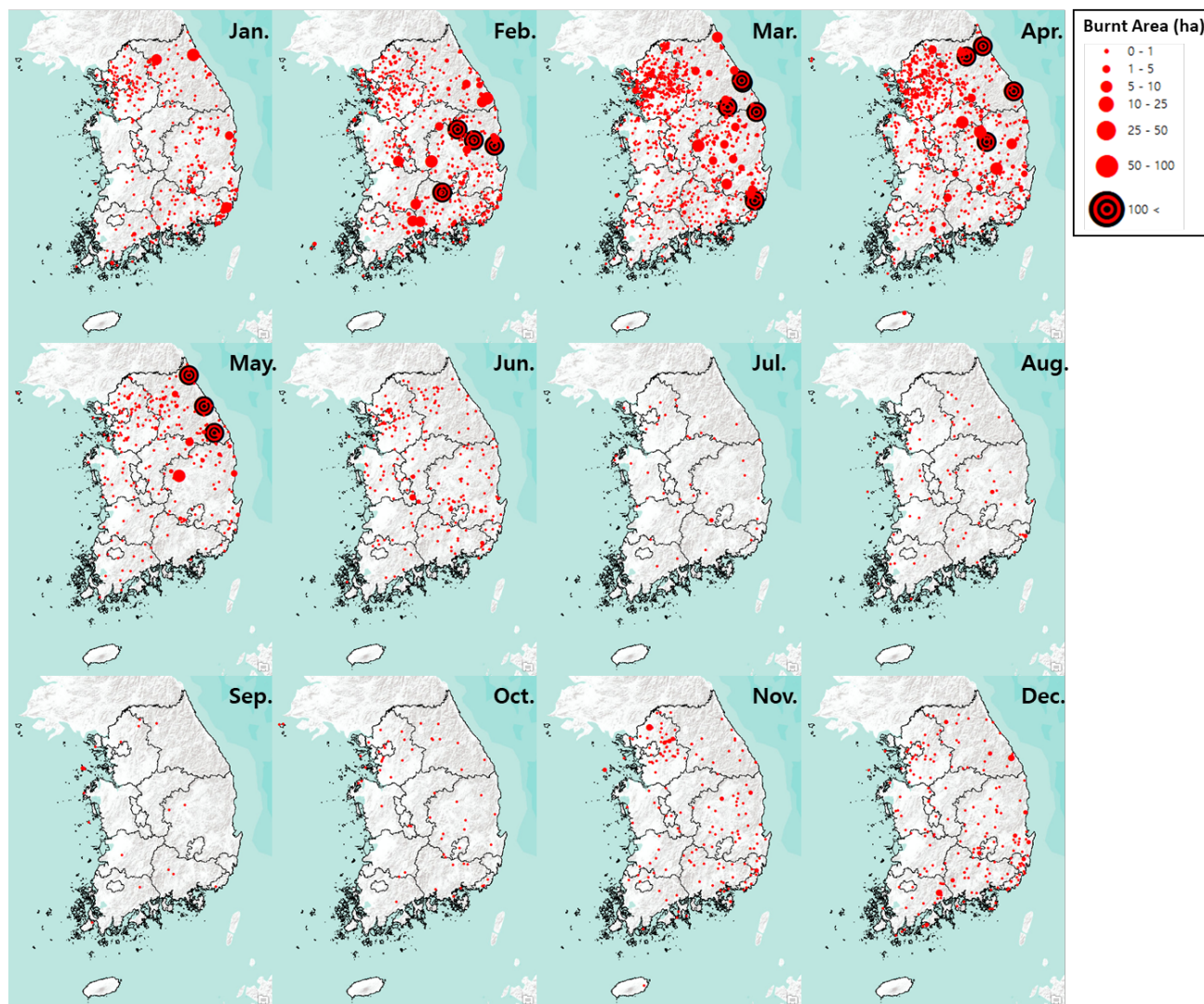
Figure 1. Patterns of forest fire frequency and scale in South Korea (from Jan. 2016 to Mar. 2022)

Materials

Forest Fire Model Developed by IIASA

The wildFire cLimate impacts and Adaptation Model (FLAM) is a process-based model developed by IIASA that contains parameterization algorithms for capturing impacts of climate, population, and fuel availability on forest fire frequency and burned area in global scale (Fig. 2). FLAM calculates ignition probability from both human and natural ignition sources by a gridded population density and monthly lightning frequency. The probability of fire is calculated by climate and fuel availability in each grid cell. The climate data is used for temperature, precipitation, wind speed, and relative humidity to compute fuel moisture content based on the Fine Fuel

Moisture Code (FFMC) of the Canadian Forest Fire Weather Index (FWI). Fuel available for burning is defined as a combination of litter and coarse woody debris (CWD) from above-ground biomass, excluding stem biomass. For the area with positive probability of fire, expected burned area is calculated by simulated fire spread based on wind speed, fuel moisture, and the fire suppression efficiency, which is implemented as the probability of extinguishing a fire on a given day in FLAM.

Figure 2. Architecture of FLAM.

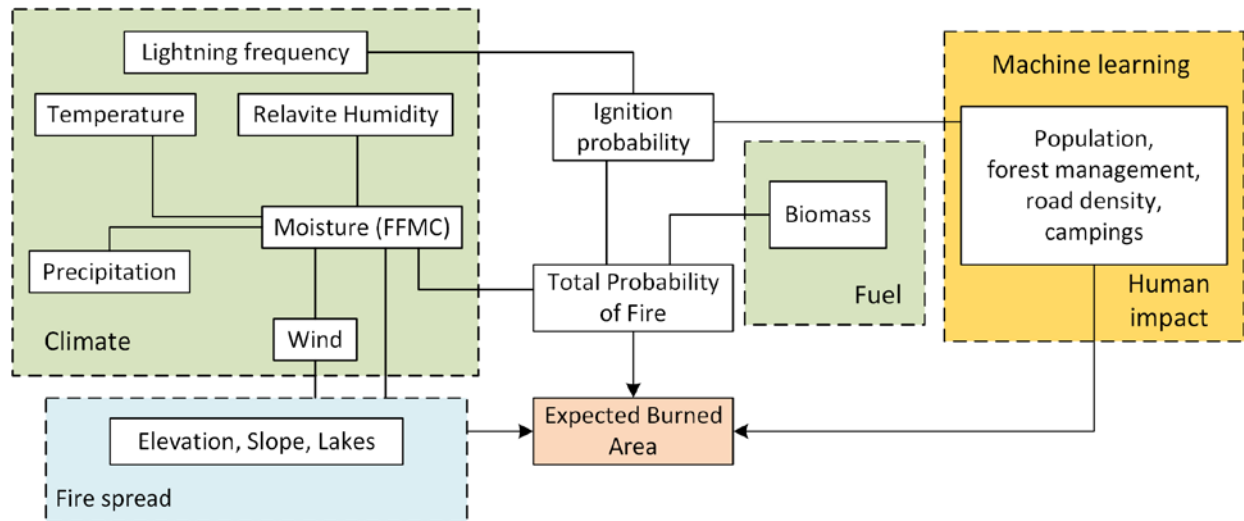One of the key features of FLAM is a procedure to calibrate spatial fire suppression efficiency for better capturing the dynamics of historical areas burned, and it can be interpreted by the effects of infrastructure and management over the processed biophysical impacts and probability of fire. Previously FLAM was more aimed to simulate burned area rather than forest fire frequency. FLAM demonstrated a good agreement of burned area in Europe and Indonesia, but these studies used global dataset lacking of forest fire frequency record (Krasovskii *et. al.*, 2016; Krasovskii *et. al.*, 2018). However, forest fire frequency is also an important feature to be related with regional environmental factors (Bergeron *et. al.,* 2004), and the impact of infrastructure and management on burned area can be better understood with an accurate projection of forest fire frequency. Therefore, this study aimed to look deeper into forest fire frequency by exploiting domestic dataset of South Korea that records each forest fire event and validate the model's applicability to the environment of Far East Asia.

Dataset Used

Forest fire dataset produced by Korea Forest Service includes burned area, start and end date of fire, ignition source, and address information for each forest fire event. In this study, the dataset was used from Jan. 2016 to Mar. 2022 where 3,511 forest fire events were found and the event locations were geo-located. Gridded population density with 1km by 1km resolution was collected from National Geographic Information Institute of Korea and the other datasets were adjusted to fit this resolution. Daily meteorological data was downloaded through API service from three different government agencies: Korea Metrological Agency (KMA), Korea Forest Research Institute, and Rural Development Agency. The data was collected from 1,209 stations covering approximately 88 km^2 of land by one station in average and interpolated for mean and max temperature,

precipitation, wind speed, and relative humidity. Lightening observation dataset produced by KMA was used to calculate lightening frequency and its processing will be explained at the following section in comparison between the preexisting and the proposed optimization method. Fuel calculation was simplified in the scale of $1km^2$ in assumption of the biomass for each grid is fully occupied by one or two out of the six dominant tree species in South Korea. Fuel is multiplication of above ground biomass (AGB) and ratio of litter and deadwood, where AGB is multiplication of stock volume, basic woody density, and biomass expansion factor (Eq.1-2).

$$Fuel = AGB * (R_t^l + R_t^d) \qquad\qquad (Eq.1)$$
$$AGB = V * WD_t * BEF_t \qquad\qquad (Eq.2)$$

AGB: Above ground biomass (t/ha) V: Stock volume (m³/ha)

R_l: Ratio of litter per AGB (Ct/ha)   WD: Basic woody density (t/m³)

R_d: Ratio of deadwood per AGB (Ct/ha)   BEF: Biomass expansion factor (unitless)

t: Pinus densiflora(Gangwon), Pinus densiflora(Midland), Pinus koraiensis,
  Larix kaempferi, Quercus variabilis, Quercus mongolica,
  Quercus variabilis and Pinus densiflora, Quercus mongolica and Pinus densiflora

Parameter V was derived from the result of Hong *et. al.* (2022), and WD, BEF, R^l, and R^d was referenced from the previous literatures including former IIASA report studied in South Korea (Lee *et. al.*, 2018; Park, 2021). Spatial distribution of agricultural land was acquired from the Farm Map which is a digitized agricultural map in parcel level produced by Ministry of Agriculture, Food and Rural Affairs. In addition, remote sensing-based land observation data was collected for land surface temperature (LST) and vegetation index from NASA Moderate Resolution Imaging Spectroradiometer (MODIS) products by using Google Earth Engine. Daily LST was acquired from MOD11A1 and masked for not clouded area with the quality band. As vegetation index changes relatively slowly compared to temperature, normalized difference vegetation index (NDVI) was acquired from MOD13A2 with 16-day composite image to minimize the noise in the time series dataset and reconstructed to daily data with the algorithm proposed by Chen *et. al.*, (2004). Aaccessible links for the used dataset can be found in the Appendix.

Methods

Ignition Probability

According to the forest fire dataset in study period, most of the forest fire had been started by human activities; 61.98% of the forest fire had been caused intentionally or mistakenly by human and 6.75% was spread from building fire. The cause of the rest 37.67% are not recorded and only 0.06% of the forest fire had been ignited by lightning. Especially, forest fire frequency is exponentially increased at near the metropolitan cities with high population density in combination with humidity lowered by multiple reasons such as urbanization, seasonal variation, and climate change (S. J. Kim *et. al.*, 2019; Sung *et. al.*, 2010). Not only in South Korea but also in Europe, human activity is a major source of forest fire (Ganteaume *et. al.*, 2013). However, unlike that European cities are highly concentrated only for small area, metropolitan cities in South Korea such as Seoul and Busan

have population densities of 15,699 and 4,320 people per km^2 respectively for each city ranges 605.2 and 770 km^2 expanding the high risk of ignition.

Therefore, we adjusted the ignition probability of FLAM to represent dominant ignition frequency at near highly populated cities. In FLAM, human impacts are modeled in combination of human ignition probability (P_h) and the suppression probability (F_{supp})

$$P_h = \min\left(1, \left(\frac{p}{p_{up}}\right)^{0.43}\right) \qquad (Eq.\,3)$$

$$F_{supp} = 1 - \left((1 - Supp_{max}) + \exp(-C_{supp} * p)\right) \qquad (Eq.\,4)$$

where p_{up}, $Supp_{max}$, and C_{supp} respectively indicates upper threshold of population density, maximum probability of instant suppression, and coefficient of population density to reach $Supp_{max}$.

In this study, P_h was optimized in the way of increasing p_{up} from the current value of 300 because it was exceeded in most of the cities accounting 7.7% of the land recording the maximum population density of 45,739 people per km^2. Meanwhile, $Supp_{max}$ and C_{supp} also have been increased from the current value of 0.9 and 0.025 to represent fast response system in South Korea that follows higher standard compared to the other countries (J. H. Kim & Lee, 2020; Scandella, 2012).

In addition to the human factor, the probability of ignition caused by lightning is currently calculated by normalizing lightning frequency in monthly time step and integrated with human factor to calculate total ignition probability as follows:

$$B_L = \max\left[0, min\left(\frac{L_f - L_{f,low}}{L_{f,up} - L_{f,low}}\right)\right], \qquad (Eq.\,5)$$

$$P_l = \frac{B_L}{B_L + \exp(1.5 - 6B_L)}, \qquad (Eq.\,6)$$

$$P_i = (P_l + (1 - P_l)P_h)(1 - F_{supp}), \qquad (Eq.\,7)$$

where L_f represents the number of flash per month in km^2 and the current value of $L_{f,low}$ and $L_{f,up}$ are 0.02 and 0.85 each. The ignition probability is then integrated with biophysical factors at the following steps to calculate probability of fire developed from the ignition. However, the current calculation process on lightening inevitably overestimates the number of forest fire caused by lightening because of the unmatched time step between lightning and the other biophysical factors in particular the fuel moisture content. As introduced above, more than 50% of the annual precipitation in South Korea is concentrated in summer. Monthly lightning frequency explodes in the rainy summer season, which rarely develops to the fire with precipitation, but when it is integrated with daily fuel moisture which is likely to include dry days in hot weather, the probability of fire will be unexpectedly increased.
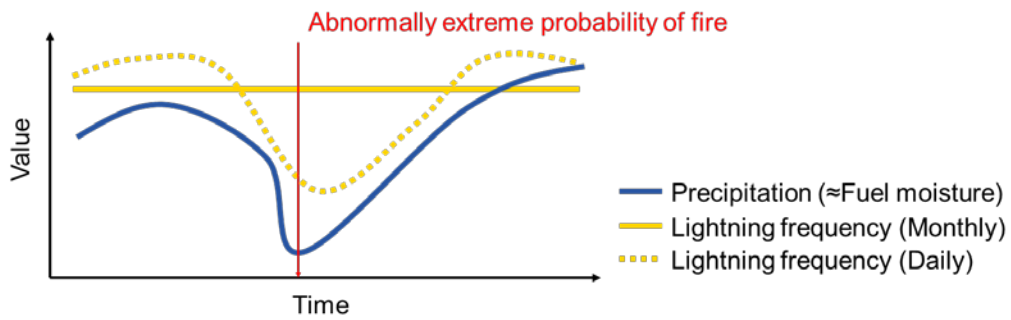
Figure 3. Conceptual illustration on extreme probability of fire
cause by the monthly calculation on lightning frequency

Therefore, the precision of lightening frequency was changed from monthly to daily time step and $L_{f,low}$ and $L_{f,up}$ were optimized for the daily B_L to have the same data distribution with monthly B_L. In addition, the number of historical forest fires caused by lightning was referenced to optimize the normalization parameters. Even though only two forest fires were recorded to be started by lightning, the parameters were optimized to return little overestimation inferring that some forest fire with unknown reason could be caused by lightning.

Warm and dry weather during spring season of South Korea results in a special pattern of forest fire that more than 60% are concentrated in a quarter of a year from Feb. to Apr. However, the skewed distribution is not only resulted from dry weather but also from the national specific custom of burning agricultural waste such as agricultural plastic waste and leftover plants after harvest. According to the dataset, 10.08% of the forest fire had been started by burning agricultural waste through the study period and the proportion increases to 22.42% when the ignition source recorded as 'burning waste' is included. Both ignition sources exponentially increase through the spring season when agricultural lands are cleaned up for the new planting, and the increasing proportion to the other ignition sources indicates that the increasing number is not solely attribute to the dry weather.
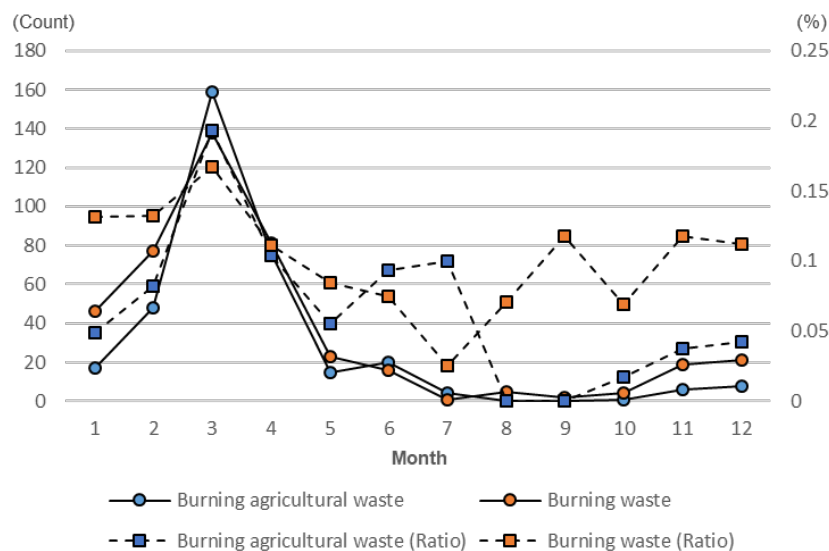

Figure 4. The number and proportion of forest fire ignited from burning (agricultural) waste

Therefore, burning agricultural waste was introduced to FLAM as a new ignition source to project the specific pattern of forest fire in South Korea. The probability of ignition from agricultural waste burning was calculated by analyzing spatial distribution of agricultural fields and fuel and weighted by the distance between them. The ignition probability after introducing the agricultural waste burning is calculated as follows:

$$P_i = (P_l + (1 - P_l)P_h + (1 - P_l - P_h)P_a + P_l P_h P_a)(1 - F_{supp}), \qquad (Eq.8)$$

where P_a is the ignition probability from agricultural waste burning.

Fuel Moisture Content Calculation

Fuel moisture content (m), calculated with daily FFMC value (V_{FFMC}) in FLAM algorithm, is one of the key factors to project both forest fire frequency and burned area (Eq.9). As a component of Canadian fire weather index (FWI), FFMC represents litter and cured fine fuel layer in top 1.2cm as an indicator of the relative ease of ignition and flammability of fine fuels (Lawson & Armitage, 2008). FFMC is calculated with daily temperature, precipitation, wind speed, relative humidity, and the m of previous day. FFMC ranges from 0 to 100 with higher value represent more flammability, and m ranges from 0 to 250% inversely proportional to FFMC (detailed formulation for FFMC be found in the appendix).

$$m = f_m(V_{FFMC}) = \frac{0.01(59.5 * 250 - 147.2 * V_{FFMC})}{V_{FFMC} + 59.5} \qquad (Eq.9)$$

In this study, daily FFMC was calculated with domestic meteorological dataset with 1km resolution enabling more precise representation on regional variations of parameter m. However, the current FFMC algorithm have limitations on acquiring additional precision and accuracy as it only exploits meteorological information without knowing the interacting land surface environment.

To overcome the limitation of meteorological modelling, Park *et. al.* (2021) proposed a framework of comparing the results of meteorological modelling and land surface observation to project future with the forecasted meteorology with calibration of empirical difference at local environment. Therefore, we also aimed to improve the calculation process of FFMC by fitting the daily parameter values m with remotely sensed soil moisture and by deriving an empirical equation of the difference that could be explained by land surface characteristics.

In this study, we compared moisture content m with Vegetation Temperature Condition Index (VTCI) which is a satellite base index effective for representing top soil moisture by interpreting LST-NDVI feature space (Wang *et. al.*, 2001). VTCI is calculated based on the ratio of LST normalized by NDVI in between upper (dry edge) and lower (wet edge) limit of the data boundary (Fig. 5). VTCI ranges from 0 to 1 for the dry and wet edge respectively corresponding to minimum and maximum evapotranspiration. Similar to FFMC representing fuel moisture content at the surface layer in top 1.2cm, VTCI is also known for reliable correlation especially with the soil moisture content in the surface level (Patel *et. al.*, 2019).
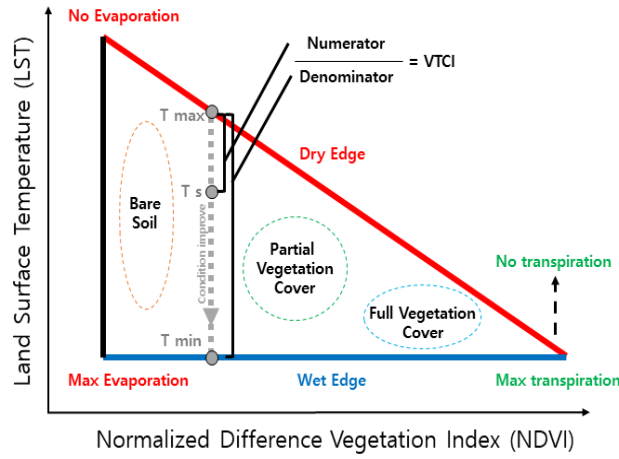
Figure 5. Concept of Vegetation Temperature Condition Index (VTCI) in LST-NDVI feature space

Considering that FFMC is calculated by integrating the meteorological condition of the day (M_t) and the previous m value (m_{t-1}), m and VTCI were compared by replacing the previous m to the previous VTCI (Eq. 10). As m and VTCI cannot be interpreted in the same scale, the iso-value lines of VTCI were optimized between the two edges. The iso-value line can both adjust the scale of VTCI and determine the way of interpreting LST-NDVI feature space so the VTCI value can better represent the moisture in specific layer (Sun, 2015), such as fuel in the surface layer.

$$m = f_m(V_{FFMC,t}) = f_m\big(f_{FFMC}(m_{t-1}, M_t)\big) \fallingdotseq f_m\left(f_{FFMC}\big(f_{iso}(V_{VTCI,t-1}), M_t\big)\right) \qquad (Eq.\,10)$$

In addition, both daily average temperature and daily maximum temperature were tested for the FFMC calculation to find which method better represents daily forest fire pattern while the original algorithm for FFMC calculation uses meteorology at noon.

Probability of Fire

Based on the ignition probability calculated from human and natural ignition sources, FLAM calculates the probability of fire – the probability of ignition develops to fire spread without instant suppression – in consideration of local biophysical factors: fuel availability and fuel moisture. However, the probability equations for integrating biophysical factors are originally designed in 1,000km^2 scale; therefore, they need to be optimized in terms of data distribution and scale when applied to 1km^2.

In the current process of FLAM, the ignition probability conditional on fuel availability (P_b) is calculated by normalizing the amount of fuel (B) as follows:

$$P_b = \max\left[0, min\left(1, \frac{B - B_l}{B_u - B_l}\right)\right], \qquad (Eq.\,11)$$

where B_u and B_l are maximum and minimum boundary of the probability set to 200 gC/m^2 and 1000 gC/m^2 as a baseline, respectively. In this study, B_u and B_l were optimized to broaden the normalization boundary as the

distribution of B will be expanded in the data with higher spatial resolution with more precise representation on environmental heterogeneity in local scale.

The daily probability of ignition by fuel moisture (P_m) is calculated by the following equation:

$$P_m = 1 - tanh\left(1.75 * \frac{m}{m_e}\right)^2, \tag{Eq. 12}$$

where m_e is the moisture of extinction set to 0.35 as a baseline. In case of the m_e, it was adjusted to reproduce the seasonal pattern of forest fire frequency in South Korea.

Then, the probability of fire (P) is calculated by the multiplication of the entire probabilities of ignition:

$$P = P_i * P_b * P_m. \tag{Eq. 13}$$

The optimization on P was performed in consideration of downscaling the data to 1km^2. As the original probability of fire (P^L) indicates probability of more than one fire in 1,000km^2, it can be expressed by the complementary event of every thousand areas consisting of the 1,000km^2 have not experienced any forest fire. Therefore, the probability of fire in 1km^2 (P^S) can be statistically derived supposing that all subordinating areas share the averaged environmental factors of the 1,000km^2. However, in practical application, P^S varies for each location because the downscaled dataset can represent heterogeneous environments, and it results in greater probability of fire as P exponentially increases at extreme environment, especially by P_m, as expressed in the following equation:

$$P^S = 1 - \sqrt[1000]{1 - (P_i * P_b * P_m)}, \tag{Eq. 14}$$

$$P^L = 1 - (1 - P^{S,Avg})^{1000} \leq 1 - \prod_{j=1}^{1000}(1 - P^{S,j}), \tag{Eq. 15}$$

where $P^{S,Avg}$ is statically downscaled P supposing that all subordinating areas share the averaged environmental factors of the 1,000km^2 and $P^{S,i}$ is statically downscaled P at the environment of location j. Therefore, to match the P^L with the integrated probability of P^S, the calculation process of P^S should be optimized by the two approaches: 1) decreasing the overall probability value or 2) producing more homogenous probability in the subordinating areas compared to the original equation. In this study, P^S was optimized by weighting the P^S of adjacent areas as a simplified method of the later approach, leaving the stepwise calibration on each probability equation as a future work. In addition, interdependency with the previous time step was introduced on P^S for modelling the recurred ignition by smouldering fire. Also, the calibration coefficient (C_{calib}) was multiplied to P for complementing the discordance between the substantial number of optimizations, such as imbalanced optimization between probability of ignition and suppression. Therefore, the optimization on P^S was performed by the following steps:

$$Step1: P^S = 1 - \sqrt[1000]{1 - (C_{calib} * P_i * P_b * P_m)}, \tag{Eq. 16}$$

$$Step\ 2: P^S = \frac{\sum_j (w_j * P^{S,j})}{\sum_j w_j}, \qquad\qquad (Eq.\,17)$$

$$Step 3: P^{S,t} = 1 - (1 - P^{S,t}) * (1 - C_{recur} * P^{S,t-1}), \qquad\qquad (Eq.\,18)$$

where j and t indicate the adjacent nine pixels in $1km^2$ resolution and projected time in daily time step, respectively, and C_{recur} represents to percentage of forest fire recurrence within one day.

Results & Discussion

Optimized Probability Equations

Table 1 shows the parameters of FLAM optimized in South Korea. According to the optimization, the probability equation at each processing step has been improved to reproduce the forest fire patterns in South Korea resulting in the changed value range. As the C_{calib} was used in this study for compensating the scale difference which is a cumulative result of probabilities caused by the original equations designed for global scale and optimization imbalances by the multicausality, probabilities are more meaningful with the interpretation of the patterns rather than the size of the values.

Table 1. FLAM Parameters Optimized in South Korea

		Human		Lightning			Fuel		Fire	
	P_{up}	$Supp_{max}$	C_{supp}	$L_{f,low}$	$L_{f,up}$	B_l	B_u	P_m	C_{calib}	C_{recur}
Global Scale	300	90	0.025	0.02	0.85	200	1,000	0.35	-	-
Optimized	2,000	94	0.100	0.02	0.55	0	2,000	0.32	30	0.0067

The human impact on forest fire ignition has been relatively increased in densely populated area by increasing the upper threshold of population density, while the probability of unsuppressed ignition in sparsely populated area has been decreased by the increased probability of instant suppression (Fig. 6).
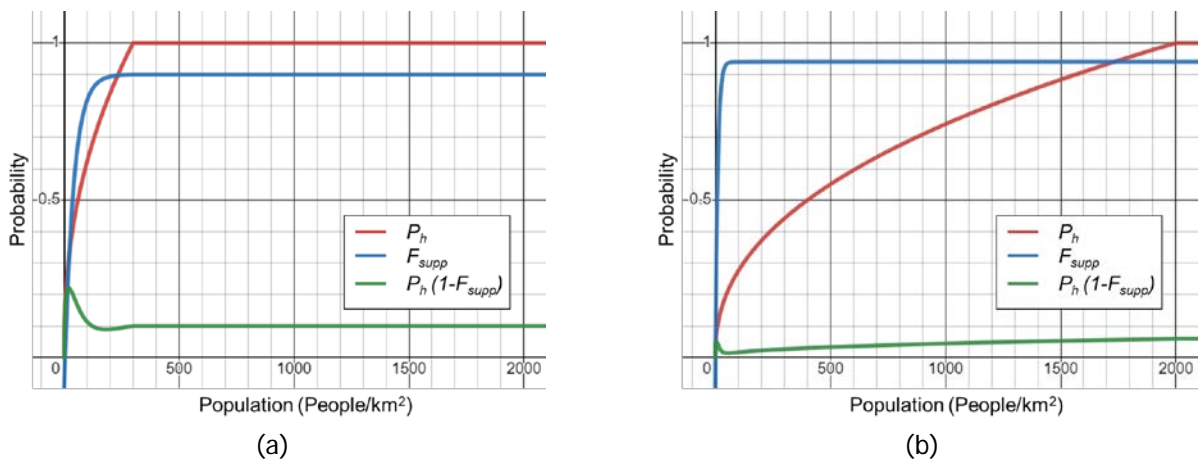

(a)   (b)

Figure 6. Optimization on ignition probability by human impact;
(a) Original probabilities in global scale, (b) Optimized probabilities in South Korea

Probability of ignition P_l was optimized in both data generation process and the equation parameters in such a way that the monthly probability has the same data distribution as the optimized daily probability (Fig. 7). As the lightening dataset is acquired for each lightning event at the exact location, lightning density was calculated with the focal statistics tool in ArcGIS software with focal radius of 17841.24m which is equivalent to 1,000km^2, as same as the designed scale of the FLAM algorithm. As a result of the optimization, the forest fire frequency ignited by lightening has been changed from 1,874.61 to 6.53 times within the study period, which corresponds to the number of observed forest fire caused by lightning.
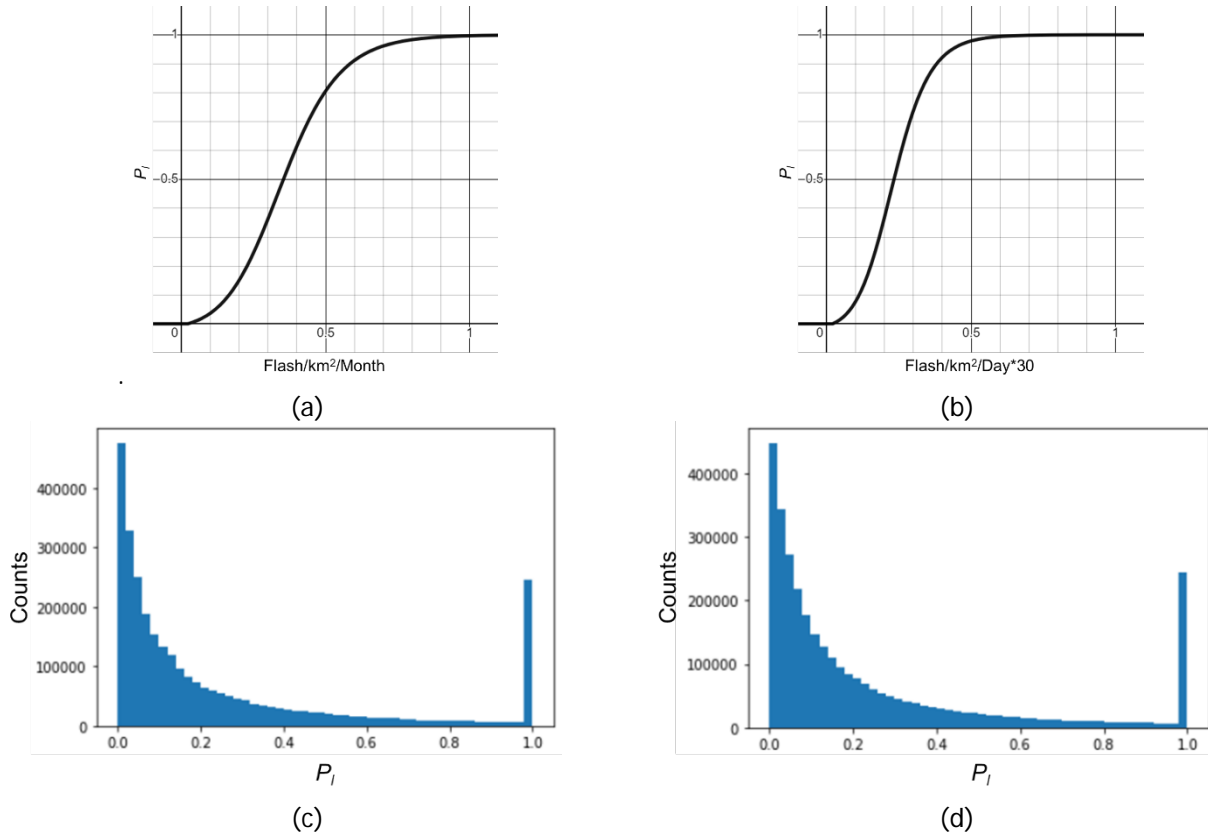

Figure 7. Optimization on ignition probability by lightning;
(a) Original probabilities in global scale, (b) Optimized probabilities in South Korea,
(c) Probability distribution calculated with monthly dataset and the original parameters,
(d) Probability distribution calculated with daily dataset and the optimized parameters

The newly introduced P_a was calculated by a function of forest boundary neighboring the agricultural field. As the calculation is processed in grid format, the number of grids with 10m resolution located at the forest boundary and neighboring agricultural field within 200m for 50m interval was acquired for each 1km^2 area (Fig. 8). Then, P_a for each 1km^2 was calculated by the following equation:

$$P_a = 1 - (1 - w_m * r_{\leq 50})^{N_{\leq 50}} * (1 - w_m * r_{\leq 100})^{N_{\leq 100}}$$
$$* (1 - w_m * r_{\leq 150})^{N_{\leq 150}} * (1 - w_m * r_{\leq 200})^{N_{\leq 200}}, \qquad \text{(Eq. 19)}$$

where $N_{\leq 50}$, $N_{\leq 100}$, $N_{\leq 150}$, and $N_{\leq 200}$ represent the number of 10m grids within 200m for 50m interval, and $r_{\leq 50}$, $r_{\leq 100}$, $r_{\leq 150}$, and $r_{\leq 200}$ are the weights for each distance set to 0.46845, 0.42829, 0.18948, and 0.13902,

respectively, referring to the forest fire ratio at each zone (Lee et. al., 2004), and w_m is weight for each month set to 3.5e-4 for Jan. and 1.2e-3 for both Feb. and Mar. based on the historical pattern of forest fire frequency.

By fitting the iso-value lines of VTCI with the Equation (10), the scale of m and VTCI have been matched in such a way that the daily fuel moisture change in both indicators roughly corresponds to each other (Fig. 9). As the two different indicators exploits different types of dataset, mismatch in local level modelling is inevitable. However, when the difference between m and VTCI is projected in the Δm - fractional vegetation cover (Fr) data space, where Fr is calculated by squared normalized NDVI (Gillies et. al., 1997), the rate of fuel moisture change was faster in the FFMC algorithm as compared to the VTCI, especially when Fr is lower and the changing amount is greater (Fig. 10); therefore, the rate of fuel moisture change in FFMC is needed to be slowed to be compatible with the remotely sensed moisture content.
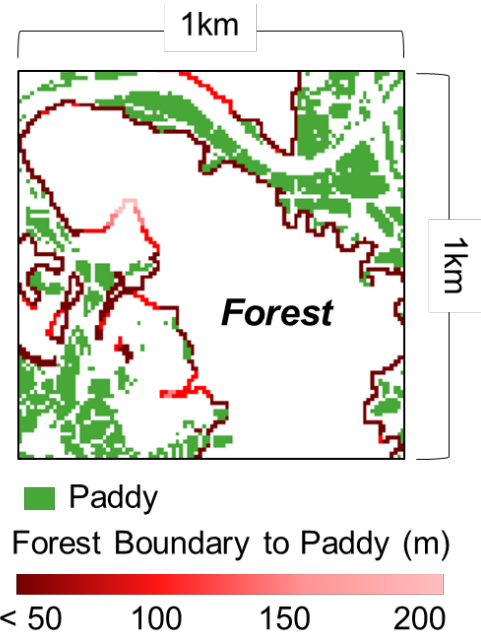

Figure 8. Counting the number of forest boundary grids neighboring agricultural field
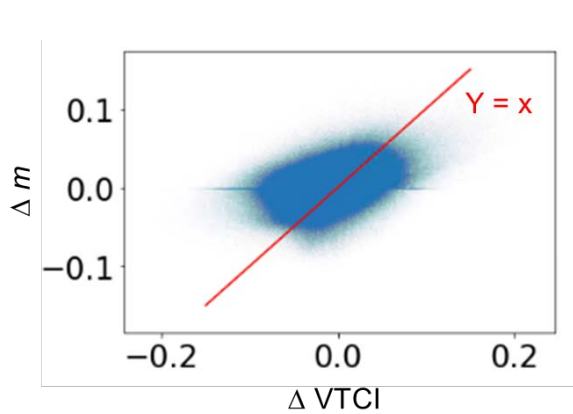

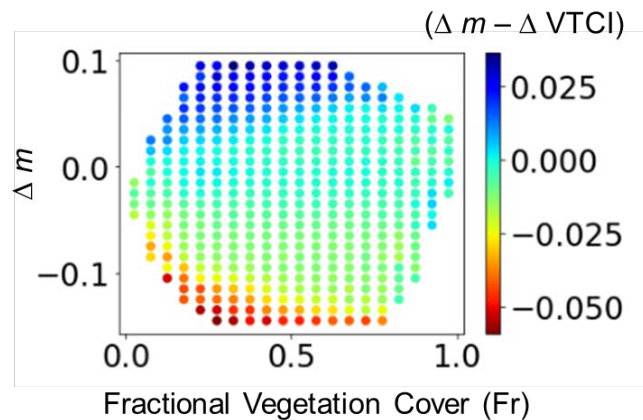*Figure 9. Comparison of daily fuel moisture change calculated by FFMC and VTCI*

Figure 10. Fuel moisture difference between FFMC and VTCI in Δm - fractional vegetation cover data space

Thus, the optimization on FFMC algorithm has been conducted by reflecting the effect of Fr and adjusting overall fuel moisture change rate. To reflect the effect of Fr on fuel moisture change rate, fine fuel equilibrium moisture content (EMC) was calibrated with the first order equation of Fr (detailed equation can be found in the appendix). As a result of optimization, higher Fr decreased EMC for drying and increased EMC for wetting, which resulted in increased change rate at higher Fr. In this stage, fuel moisture of FFMC changes faster than VTCI in both low and high Fr condition. Then, the overall fuel moisture change rate of FFMC was adjusted to 43% of the original algorithm to fit the rate with VTCI. By optimizing the algorithm with Fr, which is a representative land surface environment with simple calculation, the optimized FFMC is projectable to future with simulated Fr.

In addition, using maximum temperature for calculating m was found to be a better option for representing historical forest fire frequency pattern compared to using average temperature; it corresponds to the FFMC

calculation manual that encourages to use meteorological data at noon which is likely to be similar to the maximum temperature rather than average temperature. In the similar context, the decrement on m_e can be explained by the overestimation of m because of using daily average relative humidity.

The spatial weights at the downscaled probability of fire for increasing regional homogeneity is derived by the distance-weighted mean algorithm:

$$w_j = \frac{1}{\sum_k |d_{j,k}|}, \qquad (Eq.\ 20)$$

where k is a location of the adjacent nine pixels other than j and $d_{j,k}$ is the distance between j and k. The C_{recur} was set to 0.0067 by the percentage of historical forest fire recurrence in a day within the adjacent pixels.

Simulation on Historical Forest Fire Events

To validate the optimization performance, historical forest fire frequency and burned area were simulated by using the dataset from Jan. 2016 to Mar. 2022; the equations for burned area were not optimized in the original algorithm (Krasovskii *et. al.*, 2018). The performance was evaluated with Pearson's correlation coefficient (r) between the FLAM modelling and observed dataset, and the dataset was separated into two periods – period A and B respectively indicating before and after 2020 – to check if the model is generalized through the time.
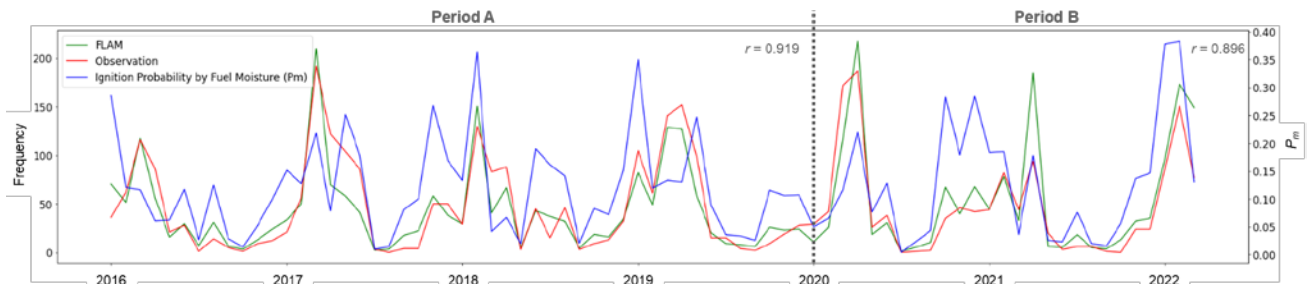

Figure 11. Temporal evaluation on forest fire frequency simulated by the optimized FLAM
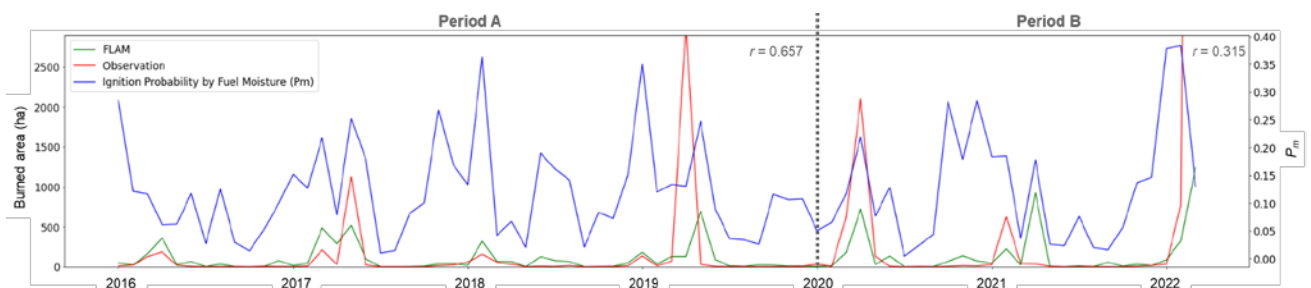
Figure 12. Temporal evaluation on burned area simulated by the optimized FLAM

According to the simulation results, temporal evaluation on forest fire frequency in period A and B has been improved from the r of 0.050 and 0.447 to 0.919 and 0.896, respectively, when the optimization condition is changed from the only application of the Equation (14) for downscaling to the full optimization (Fig. 11). Temporal evaluation on burned area was performed only for the months burned less than 1,000 ha as this study focused on frequency optimization and applied global scale optimization on burnt area. The simulation on burned area at the period A and B recorded the r of 0.657 and 0.315, respectively (Fig. 12).

The simulation on forest fire frequency was also evaluated in spatial extent by aggregating the frequency value at 25km by 25km grids. Figure. 13 shows the spatial evaluation in period A and B with the grids within 95% of confidence level recording the *r* of 0.8066 and 0.7052, respectively. The evaluation results show that the optimized FLAM is able to reproduce the forest fire patterns in South Korea showing good correlation with the historical records, particularly for the forest fire frequency. Also, the evaluation results did not show substantial difference between the period A and B; therefore, the model is expected to be robust for with respect to time periods, including possible projections of future fires. However, several outlier grids have been found in the spatial evaluation and all of the outliers were commonly underestimations in the region where high forest fire frequency was observed.

Figure 13. Spatial evaluation on forest fire frequency simulated by the optimized FLAM;
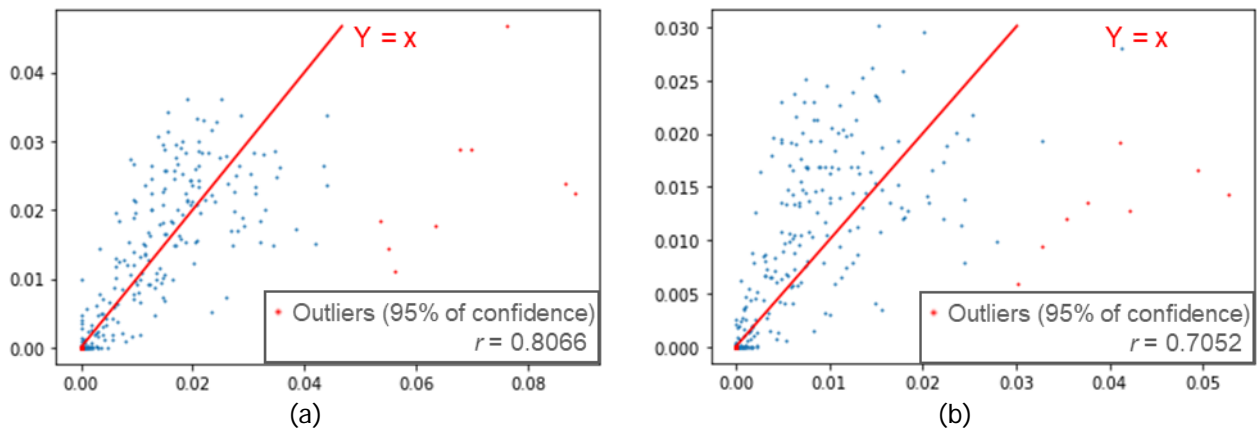(a) Period A from Jan. 2016 to Dec. 2019, (b) Period B from Jan. 2020 to Mar. 2022
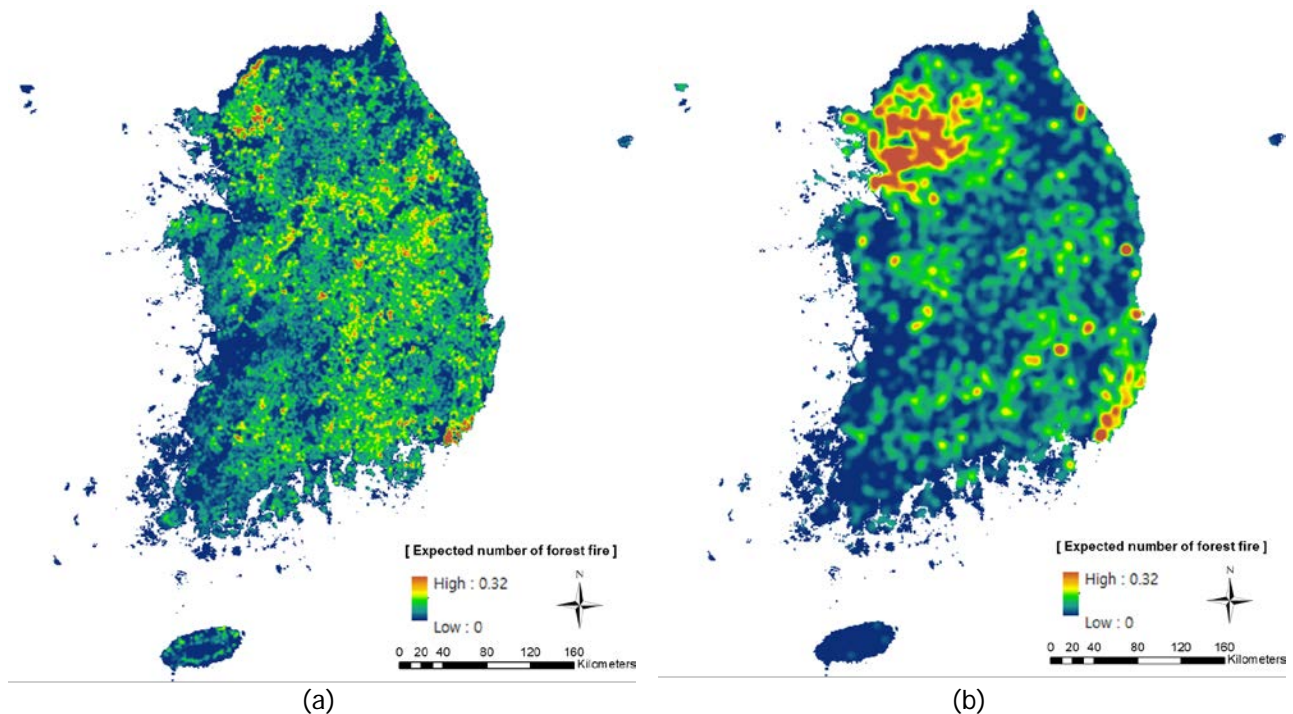

Figure 14. Expected number of forest fire through the studied period;
(a) Simulation of the optimized FLAM, (b) Observation

The underestimated forest fire frequency can be detected by comparing the maps of expected number of forest fire where the result of the optimized FLAM presents smaller scale of undispersed hotspot near the cities compared to the observation (Fig. 14). The expected number of forest fire is a cumulated sum of P which records relatively higher value through the linear feature of major mountain chains and near the cities generating varied scale of hotspot.

Discussion

In this study, probability algorithms in FLAM that works at a global scale were optimized and downscaled to the environment of South Korea to project forest fires at a local scale. The optimization was performed by using the dataset from Jan. 2016 to Mar. 2022. most of which were collected from the domestic sources and aimed at adjusting the key parameters for interpreting human and biophysical impacts on forest fires, such as population density, lightning frequency, fuel moisture, and the amount of fuel. As the previous studies on FLAM had no other choice but to focus on modelling burned area because of the limitation of using global dataset without frequency information, this study had a deeper look at the forest fire frequency which is important for interpreting forest fire ignition patterns and as an intermediate process for further improvement on burned area projection. The simulation results showed that modeling of forest fire frequency was considerably improved by the optimization from the sub-optimal evaluation score with correlation coefficient r of 0.050 and 0.447 to correlation coefficient r over 0.89, when tested for two different time periods. The simulation on burned area which has been performed without optimization of the fire spread algorithm showed a reliable correlation only for the small scale fire which is proportional to the forest fire frequency.

As the optimization process includes adjusting substantial amount of parameters for interpreting various factors, downscaling, and introducing new equations, the best optimization options were selected step by step with trial and error method aiming to reproduce historical forest fire patterns. Even though the process could handle the multiple optimization tasks efficiently and suggested overall optimization frameworks supported by background studies, further improvement on each equation is recommended to develop more effective equation forms based on the statistical analysis of forest fire patterns. For example, ignition probability by human sources needs to be improved to interpret the dispersion of human activity so the downscaled application of FLAM can reproduce large scale hotspots near the cities. In this context, C_{calib} is one of the most important factor in the current optimization process to offset the impact of accumulate error at each optimization step and represents the limitation of the current optimization process at the same time.

Although the optimization process can be further improved, the results of the optimized FLAM were promising and especially interesting, because they demonstrated the agreement between probability P_m conditional on moisture content and time-series pattern of forest fire frequency in South Korea (Fig. 11). These results show the importance of P_m on projecting forest fire frequency and also can be interpreted as an evidence of successful optimization of the FFMC algorithm. In addition, the underline hypothesis of the FFMC optimization was that the rate of soil moisture change becomes higher proportional to Fr; the hypothesis is in line with the literature that both soil moisture changes and evapotranspiration from soil were faster in forest compared to grassland (Pérez-Corona et. al., 2021; Rahgozar et. al., 2012) and that the top soil moisture content was more varied through the time when the grass coverage was higher (Yang et. al., 2019).

To further investigate the impacts of P_m in the future, the trend of the optimized P_m in spring season (Jan. and Feb.) was examined for the observed 7 years (Fig. 15). According to the result, the average P_m of the 7 years was relatively high near the Seoul metropolitan area and the east costal area, where frequent and severe forest fire currently occurs. Moreover, P_m at the east coastal area is being increased with significant level which implies that the risk of forest fire will be even more increased in the future at the areas, which have already suffered from the large-scale forest fires. Even though we may need a longer observation period to confirm this results, we are confident the risk of forest fires is being increased by the climate change with drier fuel in certain regions of South Korea.
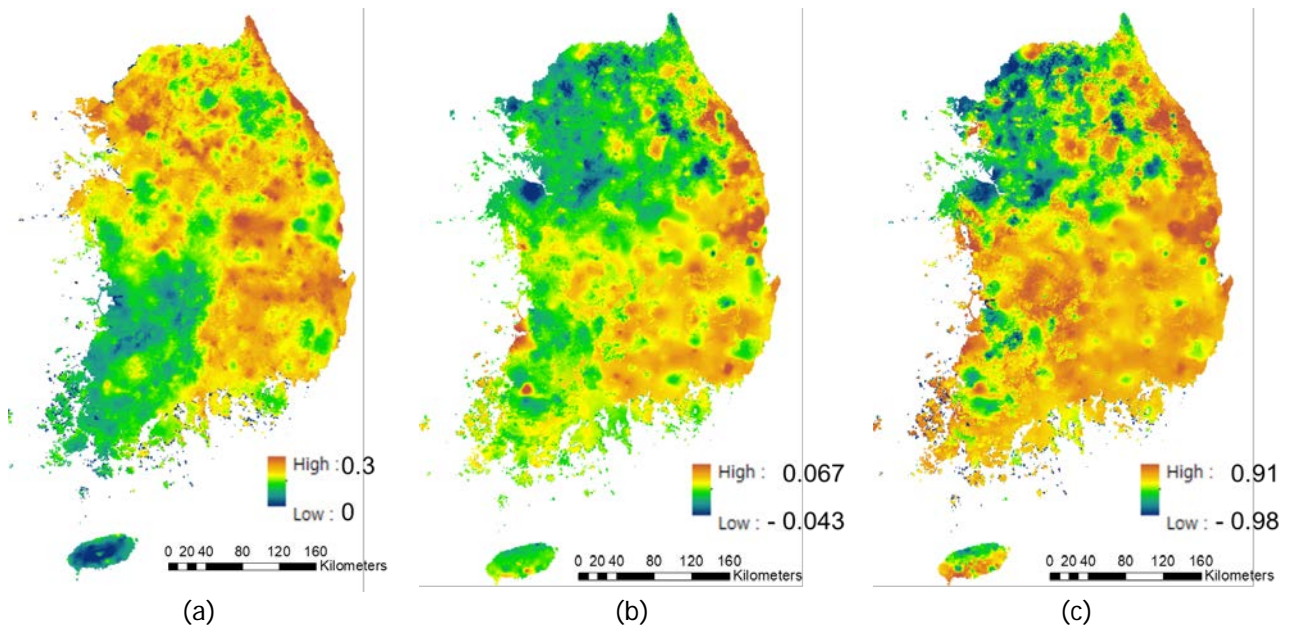

Figure 15. Trends of the ignition probability by fuel moisture (P_m) in spring season;
(a) Average P_m, (b) Slope of the time-series P_m, (c) Pearson's correlation coefficient of the time- series P_m

As a result of the optimization, FLAM can be used to project the patterns of forest fires in the future by exploiting diverse scenario dataset, which can provide useful insights for developing adaptation strategies for reducing the risk of forest fire. Therefore, we further examined its applicability on future projection by using the forest management scenario produced by Hong *et. al.* (2022). According to the projection, both forest fire frequency and burned area are expected to be increased by the increasing amount of fuel in all three future scenarios: maintaining the current management, over protection, and applying the ideal management plan based on the 6th basic forest plan of South Korea (Korea Forest Service, 2018). Nevertheless, applying the ideal forest management plan, which actively harvests wood products from over-matured forests, can decrease forest fire frequency to 63% ~ 81% of the over protection scenario and to 77% ~ 92% of remaining current management. Also, burned area can be decreased to 61% ~ 72% of the over protection scenario and to 85% ~ 96% of remaining current management.
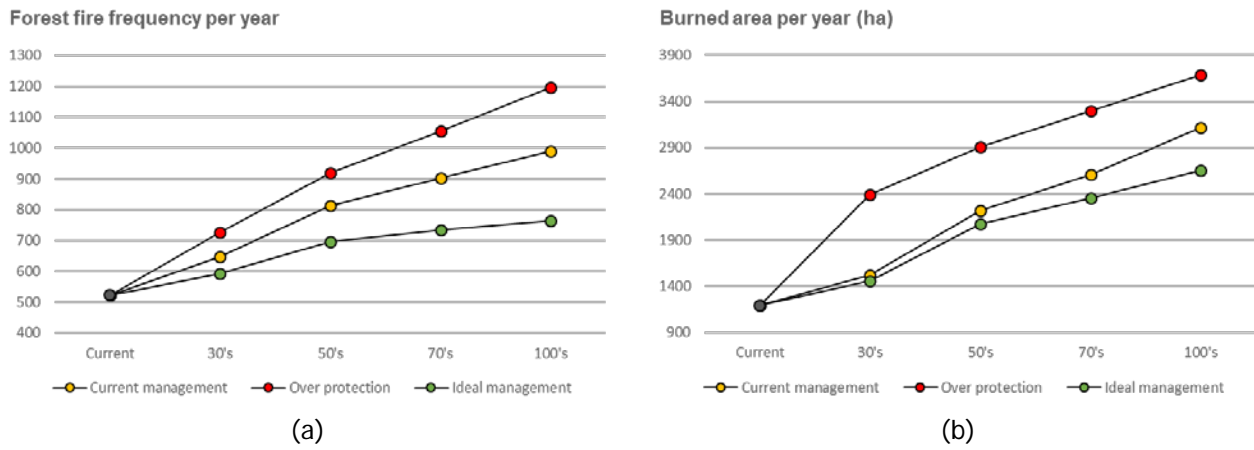
Figure 16. Future projection of forest fire by the optimized FLAM based on the forest management scenario (Hong et. al., 2022);
(a) Forest fire frequency per year, (b) Burned area per year

Conclusion and Future Work

Conclusion

In this study, we optimized FLAM to the environment of South Korea based on the national GIS data downscaled to 1km^2 resolution with additional algorithms introduced for reproducing national specific patterns of forest fire frequency, such as ignition from agricultural waste burning. For the forest fire frequency aggregated over South Korea, we obtained Pearson's correlation coefficient r of 0.893 for temporal evaluation and 0.802 for spatial evaluation which showed that the optimized FLAM is capable of capturing both spatial and temporal pattern of forest fire frequency with a reliable reproduction of the historical forest fire patterns. Considering that the pre-optimization algorithms produced sub-optimal results with r of 0.171, FLAM is applicable to South Korea only after optimization of all its modules even though it already contained main algorithms for interpreting biophysical and human impacts on forest fires at a global scale. Moreover, the limitation of the previous studies on FLAM incapable of looking deeper into the forest fire frequency, because of using global dataset, makes the optimization performed in this study valuable for the model development.

Especially, the algorithm of FFMC was improved by fitting the moisture content m to the remotely-sensed soil moisture to incorporate land surface environment in FLAM for better representation of local fuel moisture variations linked to vegetation. With the improved algorithms, time-series pattern of probability P_m conditional on moisture content showed good agreement with the seasonal patterns of the forest fire frequency. Meanwhile, based on the simulated forest fire frequency, dense population in urbanized area in combination with other factors lead to exponentially increasing probability of fire. In this context, P_m seems to be the most plausible factor for exploding forest fire in the future as the increasing trend of P_m put additional threats to the already affected areas, which can be interpreted as a result of a changing climate.

Future Work

As the optimization succeeded to reproduce the national specific pattern of forest fire in South Korea, it should be followed by the research on developing adaptation strategies for reducing forest fire risks with diverse application of the future scenarios' dataset. This study has already presented a future projection by using forest management scenario which showed the effect of ideal forest management reducing approximately a quarter of forest fire frequency. Therefore, the following task will aim at finding the best adaptation scenario by integrating climate change scenarios dataset with multiple adaptation options in consideration of feasibility, cost effectiveness, regional priority, etc.

In this context, FLAM that currently works with probabilities can be modified to the agent-based-model (ABM) to better identify the tipping point or threshold that provokes extreme forest fire events. For example, if the fire spread algorithm of FLAM are converted to the ABM and reflects the limited suppression capability in the algorithms, the burned areas caused by the large scale forest fires can be estimated better as unsuppressed fire spreading between the adjacent pixels and modelled by as the interactions between agents. Inversely, the demanded suppression capability can be forced to minimize forest fire damage in various climate change scenarios.

References

Sutanto, S. J., Vitolo, C., Di Napoli, C., D'Andrea, M., & Van Lanen, H. A. (2020). Heatwaves, droughts, and fires: Exploring compound and cascading dry hazards at the pan-European scale. Environment international, 134, 105276.

Clark, J. S., Royall, P. D., & Chumbley, C. (1996). The role of fire during climate change in an eastern deciduous forest at Devil's Bathtub, New York. Ecology, 77(7), 2148-2166.

Randerson, J. T., Liu, H., Flanner, M. G., Chambers, S. D., Jin, Y., Hess, P. G., ... & Zender, C. S. (2006). The impact of boreal forest fire on climate warming. science, 314(5802), 1130-1132.

Engle, N. L., de Bremond, A., Malone, E. L., & Moss, R. H. (2014). Towards a resilience indicator framework for making climate-change adaptation decisions. Mitigation and Adaptation Strategies for Global Change, 19(8), 1295-1312.

Gavin, D. G., Hallett, D. J., Hu, F. S., Lertzman, K. P., Prichard, S. J., Brown, K. J., ... & Peterson, D. L. (2007). Forest fire and climate change in western North America: insights from sediment charcoal records. Frontiers in Ecology and the Environment, 5(9), 499-506.

Fernandez-Anez, N., Krasovskiy, A., Müller, M., Vacik, H., Baetens, J., Hukić, E., ... & Cerda, A. (2021). Current wildland fire patterns and challenges in Europe: A synthesis of national perspectives. Air, Soil and Water Research, 14, 11786221211028185.

Varela, V., Vlachogiannis, D., Sfetsos, A., Karozis, S., Politi, N., & Giroud, F. (2019). Projection of Forest Fire Danger due to Climate Change in the French Mediterranean Region. Sustainability 2019, 11, 4284.

Jadmiko, S. D., Murdiyarso, D., & Faqih, A. (2017, March). Climate changes projection for land and forest fire risk assessment in West Kalimantan. In IOP Conference Series: Earth and Environmental Science (Vol. 58, No. 1, p. 012030). IOP Publishing.

Korea Forest Service. (2022). Yearbook of Forest Fire Statistics, Association Together with the Disabled (Online publication available at https://www.forest.go.kr/kfsweb/cmm/fms/FileDown.do?atchFileId=FILE_000000020067170&fileSn=1&dwldHistYn=Y&bbsId=BBSMSTR_1008)

Lim, C. H., Kim, Y. S., Won, M., Kim, S. J., & Lee, W. K. (2019). Can satellite-based data substitute for surveyed data to predict the spatial probability of forest fire? A geostatistical approach to forest fire in the Republic of Korea. Geomatics, Natural Hazards and Risk, 10(1), 719-739.

Lee, J. G., & In, S. R. (2009). A numerical sensitivity experiment of the downslope windstorm over the Yeongdong region in relation to the inversion layer of temperature. Atmosphere, 19(4), 331-344.

Sung, M. K., Lim, G. H., Choi, E. H., Lee, Y. Y., Won, M. S., & Koo, K. S. (2010). Climate change over Korea and its relation to the forest fire occurrence. Atmosphere, 20(1), 27-35.

Krasovskii, A., Khabarov, N., Migliavacca, M., Kraxner, F., & Obersteiner, M. (2016). Regional aspects of modelling burned areas in Europe. International Journal of Wildland Fire, 25(8), 811-818.

Krasovskii, A., Khabarov, N., Pirker, J., Kraxner, F., Yowargana, P., Schepaschenko, D., & Obersteiner, M. (2018). Modeling burned areas in Indonesia: The FLAM approach. Forests, 9(7), 437.

Bergeron, Y., Flannigan, M., Gauthier, S., Leduc, A., & Lefort, P. (2004). Past, current and future fire frequency in the Canadian boreal forest: implications for sustainable forest management. AMBIO: A Journal of the Human Environment, *33*(6), 356-360.

Hong, M., Song, C., Kim, M., Kim, J., Lee, S. G., Lim, C. H., ... & Lee, W. K. (2022). Application of integrated Korean forest growth dynamics model to meet NDC target by considering forest management scenarios and budget. *Carbon Balance and Management*, *17*(1), 1-18.

Lee, S. J., Yim, J. S., Son, Y. M., Son, Y., & Kim, R. (2018). Estimation of forest carbon stocks for national greenhouse gas inventory reporting in South Korea. *Forests*, *9*(10), 625.

Park, E. (2021). Assessment of Afforestation Options with Special Emphasis on Forest Productivity and Carbon Storage in North Korea. Retrieved from https://pure.iiasa.ac.at/id/eprint/17471/

Chen, J., Jönsson, P., Tamura, M., Gu, Z., Matsushita, B., & Eklundh, L. (2004). A simple method for reconstructing a high-quality NDVI time-series data set based on the Savitzky–Golay filter. *Remote sensing of Environment*, *91*(3-4), 332-344.

Kim, S. J., Lim, C. H., Kim, G. S., Lee, J., Geiger, T., Rahmati, O., ... & Lee, W. K. (2019). Multi-temporal analysis of forest fire probability using socio-economic and environmental variables. *Remote Sensing*, *11*(1), 86.

Ganteaume, A., Camia, A., Jappiot, M., San-Miguel-Ayanz, J., Long-Fournel, M., & Lampin, C. (2013). A review of the main driving factors of forest fire ignition over Europe. *Environmental management*, *51*(3), 651-662.

Kim, J. H., & Lee, H. J. (2020). Study on Cases of Priority Traffic Signal System for Emergency Vehicles: Based on a City's Pilot Operation Cases in Chungcheongbukdo Province. *Fire Science and Engineering*, *34*(1), 121-126.

Scandella, F. (2012). *Firefighters: feeling the heat*. Brussels, Belgium: European Trade Union Institute.

Lawson, B. D., & Armitage, O. B. (2008). *Weather Guide for the Canadian Forest Fire Danger Rating System*. Natural Resources Canada, Canadian Forest Service, Northern Forestry Centre, Edmonton, Alberta.

Park, E., Jo, H. W., Lee, W. K., Lee, S., Song, C., Lee, H., ... & Kim, T. H. (2022). Development of earth observational diagnostic drought prediction model for regional error calibration: A case study on agricultural drought in Kyrgyzstan. *GIScience & Remote Sensing*, *59*(1), 36-53.

Wang, P. X., Li, X. W., Gong, J. Y., & Song, C. (2001, July). Vegetation temperature condition index and its application for drought monitoring. In *IGARSS 2001. Scanning the Present and Resolving the Future. Proceedings. IEEE 2001 International Geoscience and Remote Sensing Symposium (Cat. No. 01CH37217)* (Vol. 1, pp. 141-143). IEEE.

Patel, N. R., Mukund, A., & Parida, B. R. (2022). Satellite-derived vegetation temperature condition index to infer root zone soil moisture in semi-arid province of Rajasthan, India. *Geocarto International*, *37*(1), 179-195.

Sun, H. (2015). Two-stage trapezoid: A new interpretation of the land surface temperature and fractional vegetation coverage space. *IEEE Journal of Selected Topics in Applied Earth Observations and Remote Sensing*, *9*(1), 336-346.

Lee, S. Y., An, S. H., Won, M. S., Lee, M. B., Lim, T. G., & Shin, Y. C. (2004). Classification of forest fire occurrence risk regions using GIS. *Journal of the Korean Association of Geographic Information Studies*, *7*(2), 37-46.

Gillies, R. R., Kustas, W. P., & Humes, K. S. (1997). A verification of the'triangle'method for obtaining surface soil water content and energy fluxes from remote measurements of the Normalized Difference Vegetation Index (NDVI) and surface e. *International journal of remote sensing*, *18*(15), 3145-3166.

Pérez-Corona, M. E., Pérez-Hernández, M. D. C., Medina-Villar, S., Andivia, E., & Bermúdez de Castro, F. (2021). Canopy species composition drives seasonal soil characteristics in a Mediterranean riparian forest. *European Journal of Forest Research*, *140*(5), 1081-1093.

Rahgozar, M., Shah, N., & Ross, M. (2012). Estimation of evapotranspiration and water budget components using concurrent soil moisture and water table monitoring. *International Scholarly Research Notices*, *2012*.

Yang, W., Wang, Y., He, C., Tan, X., & Han, Z. (2019). Soil water content and temperature dynamics under grassland degradation: a multi-depth continuous measurement from the agricultural pastoral ecotone in Northwest China. Sustainability, 11(15), 4188.

Korea Forest Service. 2018. The 6th basic forest plan (2018~2037). Daejeon: Korea Forest Service. pp. 151.

Appendix

Dataset Used

Table 2. Source of the dataset used

Dataset	Source
Forest Fire Dataset	https://www.data.go.kr/data/3062614/openapi.do
Gridded Population Density	http://map.ngii.go.kr/ms/map/NlipMap.do?tabGb=total
Meteorological Dataset	https://data.kma.go.kr/data/grnd/selectAsosRltmList.do?pgmNo=36
Farm Map	http://data.nsdi.go.kr/dataset/20210707ds00001
MOD11A1	https://developers.google.com/earth-engine/datasets/catalog/MODIS_061_MOD11A1
MOD13A2	https://developers.google.com/earth-engine/datasets/catalog/MODIS_061_MOD13A2

FFMC Algorithms

r_o, T, H, W respectively indicate precipitation, temperature, relative humidity, and wind speed. F_o is FFMC value at the previous day and E_d and E_w respectively indicates EMC for drying and EMC for wetting. Equations starting with ▷ symbol only work for the optimization while equations starting with ▶ symbol do not applied to the optimization. Optimization parameters w_1, w_2, w_3, and $w4$ were respectively set to 0.621, 0.338, 0.994, and 0.43 by the minimizing the fitting error, and they may not follow natural phenomenon; therefore, they should be carefully applied to the other dataset.

$$m_o = 47.2(101 - F_o)/(59.5 + F_o)$$

$$r_f = r_o - 0.5 \quad if \ r_o > 0.5$$

$$m_r = m_o + 42.5 r_f (e^{-100/(251-m_o)})(1 - e^{-6.93/r_f}) \quad if \ m_o \leq 150$$

$$m_r = m_o + 42.5 r_f (e^{-100/(251-m_o)})(1 - e^{-6.93/r_f}) + 0.0015(m_o - 150)^2 r_f^{0.5} \quad if \ m_o > 150$$

$$m_o = m_r$$

$$E_d = 0.942 H^{0.679} + 11 e^{(H-100)/10} + 0.18(21.1 - T)(1 - e^{-0.115H})$$

$$E_w = 0.618 H^{0.753} + 10 e^{(H-100)/10} + 0.18(21.1 - T)(1 - e^{-0.115H})$$

$$\triangleright E_d = E_d - (w_1 F r^{w_2} + w_3)$$

$$\triangleright E_w = E_w + (w_1 F r^{w_2} + w_3)$$

$$k_o = 0.424[1 - (H/100)^{1.7}] + 0.0694W^{0.5}[1 - (H/100)^8]$$

$$k_d = k_o * 0.581e^{0.0365T}$$

$$k_l = 0.424[1 - ((100 - H)/100)^{1.7}] + 0.0694W^{0.5}[1 - ((100 - H)/100)^8]$$

$$k_w = k_l * 0.581e^{0.0365T}$$

$\blacktriangleright$ $m = E_d + (m_o - E_d) * 10^{-k_d}$ $if \ m_o > E_d \ else,$

$\blacktriangleright$ $m = E_w + (E_w - m_o) * 10^{-k_w}$ $if \ m_o < E_w \ else,$

$\triangleright$ $m = (1 - w_4)m_o + w_4[E_d + (m_o - E_d) * 10^{-k_d}]$ $if \ m_o > E_d \ else,$

$\triangleright$ $m = (1 - w_4)m_o + w_4[E_w + (E_w - m_o) * 10^{-k_w}]$ $if \ m_o < E_w \ else,$

$m = m_o$